The Phantom Laboratory + image Owl

Magphan® RT

Precision QA for MR

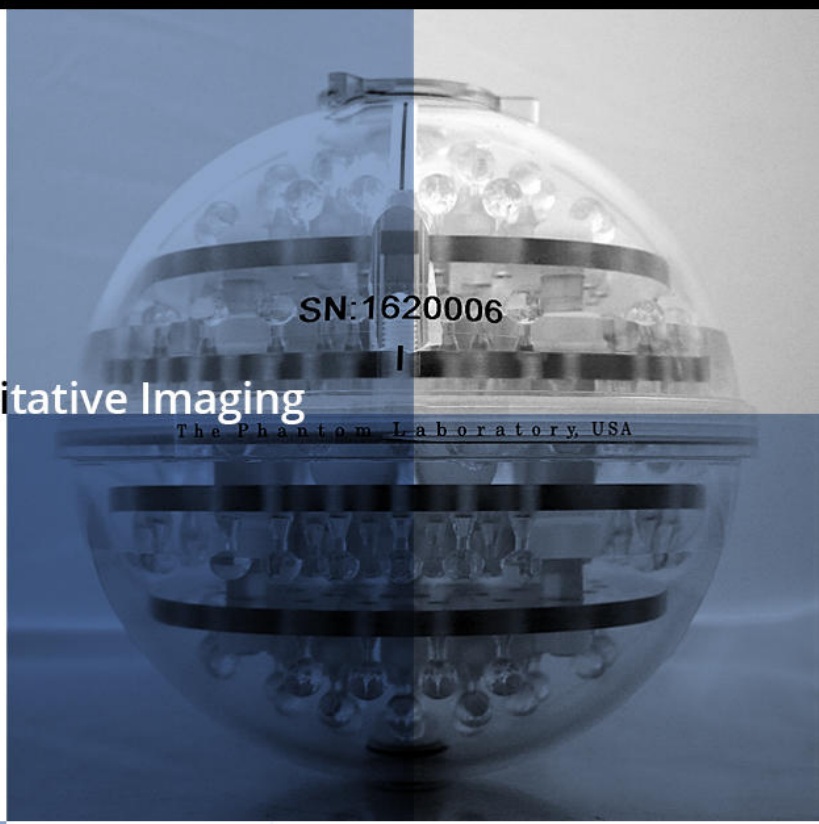

MR QA for Radiotherapy and Quantitative Imaging

Magphan® head and body phantoms address the needs for precise measurements of quantitative MR. The phantoms are supplied with two years of Image Owl's high-powered automated analysis.

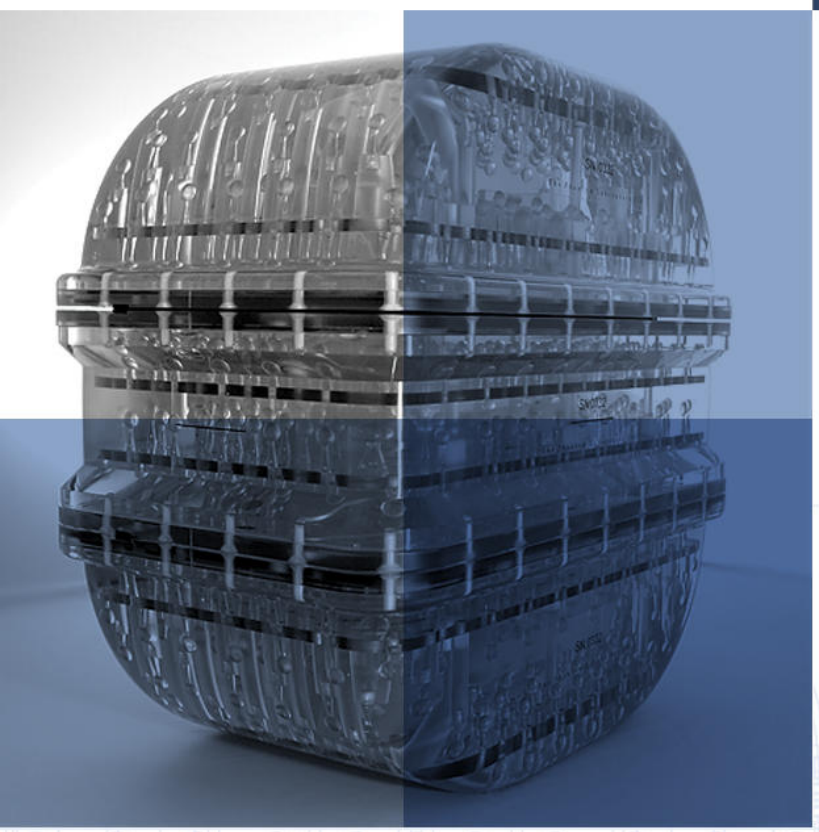

In addition to accurate sub-millimeter distortion measurements, Magphan phantoms include tests for high resolution, slice geometry, noise, uniformity and more. Because it is critical to test the actual image parameters you are using, the phantom is designed to work with a wide range of clinical protocols.

Contact us today for a demo and discussion of your MR QA requirements.

info@phantomlab.com
518-692-1190

Analysis of noise in phase contrast MR imaging

A. H. Andersen[a] and J. E. Kirsch
Magnetic Resonance Imaging and Spectroscopy Center, Department of Diagnostic Radiology, University of Kentucky, Lexington, Kentucky 40536

(Received 12 June 1995; accepted for publication 21 March 1996)

In this work we analyze the effects of inherent random noise on the detectability of low-contrast vessel structures that possess slow flow. When flow is encoded in more than one direction, the number of independent noise contributions increases in addition to the scan time. In a fast-flow scenario, only the noise contribution from sampling along the direction of flow is of any significance. At slow flow rates, however, it becomes necessary to account for the noise in each encoded Cartesian direction. The degree to which noise affects low-contrast detectability also depends on the method of phase contrast image processing employed. A theoretical analysis of the statistical properties of signal and noise in processed phase contrast magnitude images is presented and verified from experimental MR image data. Results show a progressively increased bias in the processed phase contrast image magnitude at slow flow rates due to contributions from inherent random noise. The amount of this bias increases with the number of physical directions in which flow is encoded and is larger for complex difference processed images than for phase difference processing. Correspondingly, the output signal-to-noise ratio associated with flow is compromised.

Key words: noise, magnetic, resonance, imaging, flow

I. INTRODUCTION

Phase contrast magnetic resonance (MR) imaging techniques have been widely reported.[1–11] In a flow-sensitized image, spins moving in the presence of magnetic field gradients obtain a different phase than static spins. The phase contrast effect is achieved when a flow-compensated image is subtracted so as to cancel the incidental fluctuations in phase associated with field inhomogeneities, etc. and unrelated to flow. Motion in all directions has been studied with six-point methods, where each pair of images depict motion along one of three orthogonal Cartesian directions.[3] Most work has focused on effects primarily associated with fast flow.[12,13] The statistical description of the effects of noise also has been mostly limited to fast flow, where the signal-to-noise ratio of the processed vascular image is high.[2,8,11,14–18] At high flow rates, only the noise component aligned with the direction of flow contributes to the processed vector magnitude. This is equivalent to a scenario in which the direction of flow is known *a priori* and encoding is limited to that direction. The noise can then be considered additive white zero-mean Gaussian with a standard deviation that is invariant to the number of directions of flow encoding as well as to the type of phase contrast image processing employed.

Fast flow, however, is not a particularly interesting scenario as far as phase contrast MR image processing and detectability in the context of inherent system noise uncorrelated to the signal is concerned. An important challenge in phase contrast imaging lies in our ability to use these techniques to detect small vessels having slow flow. That is, we need to develop an apparatus that can adequately characterize the statistical properties of and subsequently the detectability of image voxels in which the signal level associated with blood flow is approaching the inherent noise level. We present here a complete statistical description of the interaction between the phase contrast signal and uncorrelated random noise that is valid for all rates of flow. This description shows the nonlinear threshold effect that comes into play at low levels of the phase contrast image signal-to-noise ratio as well as the dependence on the number of noise component contributions through the number of directions of flow encoding and the type of image processing employed.

At present, the statistical description is available to fully characterize the probability distribution of signal plus noise only for flow encoding in one direction with complex difference processing and for flow encoding in up to two directions with phase difference processing.[26] Both imaging situations involve noise having at most two degrees of freedom. For phase difference processing, when the magnitude of encoded and unencoded voxels is large relative to the noise standard deviation, the phase difference will have a Gaussian noise distribution for each encoding direction. For complex difference processing, regardless of the image voxel magnitude, real and imaginary channels for each encoding direction will have Gaussian noise distributions. The statistical description of the magnitude of two independent Gaussian random variables that are in phase quadrature was developed initially by Rice.[19] The associated probability density function is commonly referred to as Rician and is widely encountered in communication theory.[26] In the context of MR imaging, the effect of independent Gaussian noise in real and imaginary channels on conventional magnitude reconstructed images is fully characterized by this distribution. Early work addressed the importance of noise calibration.[20,21] Also, the advantage of phase-corrected real over magnitude reconstructed images has been the focus of a considerable amount

 0094-2405/96/23(6)/857/13/$10.00

of effort.[22] Of particular relevance to phase contrast imaging is the discussion of homodyne (coherent) versus magnitude (envelope) detection.[23] These efforts all have made use of the explicit form of the Rician probability density function.

Whereas, in communication theory, the encounter of Gaussian noise of dimension higher than two is limited to seemingly more esoteric subjects,[24,25] such higher dimensions are a tangible feature of MR angiography. In three-dimensional (3-D) imaging of flow, velocity can be encoded in up to three orthogonal physical directions. The signal associated with each direction is complex, consisting of real and imaginary channels. Since the measurements are statistically independent, we need to characterize the interaction of signal and random noise components in hyperspaces of order up to six. The four-point method for which the use of a common flow-compensated acquisition leads to noise contributions that are correlated between the three Cartesian directions is considered here only in the context of simulation studies of signal corrupted by computer-generated random Gaussian noise.

II. PHASE CONTRAST IMAGE FORMATION

Phase contrast MR imaging is an enhancement procedure by which signal contributions from stationary tissue are suppressed through post-processing using some method of subtraction. The calculations typically start with pairs of complex-valued base images, although in principle homodyne detection could also be used.[23] One image is obtained from an experiment in which a bipolar gradient pulse is being used for encoding of flow in what one may arbitrarily refer to as the positive direction. The other image is either a flow-compensated reference image or is obtained using an opposite bipolar gradient pulse for encoding of negative flow. One such pair of images is acquired for each of up to three orthogonal directions of flow encoding. Motion in all Cartesian directions can be studied with six-point methods. Phase contrast enhancement is achieved by either phase difference or complex difference processing of the complex-valued base images. The subtraction is performed on a pixel-by-pixel basis for each slice. We use $\mathbf{S}_+$ and $\mathbf{S}_-$ to denote the complex-valued amplitude of a particular pixel in positive- and negative-encoded base images, respectively. The complex amplitude $\mathbf{S}_\pm$ is made up from a deterministic (signal) component $A_\pm e^{i(\phi_0 \pm \Delta\phi)}$ pertaining to flow and additive zero-mean Gaussian random quadrature noise components $\mathbf{n}_{r\pm}$ and $\mathbf{n}_{i\pm}$ of equal variance σ_n^2 in real and imaginary channels. ϕ_0 is the uncontrollable incidental phase component associated primarily with field nonuniformity and which is assumed to be present in both complex base images $\mathbf{S}_+$ and $\mathbf{S}_-$; $\Delta\phi$ is the additional phase associated with the encoding of flow:

$$\begin{aligned} \mathbf{S}_+ &= A_+ e^{i(\phi_0+\Delta\phi)} + \mathbf{n}_{r_+} + i\mathbf{n}_{i_+}, \\ \mathbf{S}_- &= A_- e^{i(\phi_0-\Delta\phi)} + \mathbf{n}_{r_-} + i\mathbf{n}_{i_-}. \end{aligned} \tag{1}$$

Disregarding partial voluming effects, we can consider voxels in separate base images to have equal magnitudes, i.e., $A_+ = A_- = A$. It should be noted that this approximation may hold more accurately when symmetric flow encoding is used, due to intravoxel and/or view-to-view effects.

A. Phase difference calculation

The magnitude-weighted phase difference image[8] $\mathbf{S}_{\mathrm{PD}}$ is calculated as

$$\mathbf{S}_{\mathrm{PD}} = \frac{|\mathbf{S}_+| + |\mathbf{S}_-|}{2} [\angle\mathbf{S}_+ - \angle\mathbf{S}_-]_{2\pi}, \tag{2}$$

where $[\cdot]_{2\pi}$ implies subtraction modulo 2π. (Modulo 2π phase subtraction is equivalent to multiplication by the complex conjugate.) With $A_+ = A_- = A$, the deterministic signal component of the phase-difference processed image becomes $2A\Delta\phi$. When the phase difference is computed modulo 2π, we need not be concerned with wrap of the separate phase components $\angle\mathbf{S}_+$ and $\angle\mathbf{S}_-$. Phase unwrapping can then be avoided as long as the phase *difference* $2\Delta\phi$ is limited to the principal range $[-\pi,\pi[$. In fact, our analysis focuses on slow-flow scenarios for which $\Delta\phi < 1$. When we assume that $A_+ = A_- = A$ and ignore the contribution from noise in the average magnitude image mask, the phase contrast image obtained by phase difference processing will be of the form

$$\mathbf{S}_{\mathrm{PD}} = A[2\Delta\phi + (\mathbf{n}_{\phi_+} - \mathbf{n}_{\phi_-})], \tag{3}$$

where $\mathbf{n}_{\phi+}$ and $\mathbf{n}_{\phi-}$ are independent zero-mean Gaussian noise components of equal standard deviation σ_n/A.[15,26] Thus, this is a setting of order $N=1$ for which the total additive random noise component $A(\mathbf{n}_{\phi+} - \mathbf{n}_{\phi-})$ of the magnitude-weighted phase difference image will be a zero-mean Gaussian of variance $2\sigma_n^2$. Equation (3) is valid when the base image signal-to-noise ratio $A/\sigma_n \gg 1$ and $\Delta\phi$ is small so that we may ignore the contribution from noise in the magnitude mask. In the air background, the phase noise is uniform on the interval $[-\pi,\pi[$.

B. Complex difference calculation

The magnitude of the complex difference yields an image $\mathbf{S}_{\mathrm{CD}}$,

$$\mathbf{S}_{\mathrm{CD}} = |\mathbf{S}_+ - \mathbf{S}_-|. \tag{4}$$

With $A_+ = A_- = A$, the deterministic signal component of the complex-difference processed image becomes $2A|\sin\Delta\phi|$. Again, since we are primarily interested in $\Delta\phi < 1$, there is no wrap of the phase difference and $\sin\Delta\phi$ is unique as well. When Eq. (1) is used to express each of the complex-valued base images $\mathbf{S}_+$ and $\mathbf{S}_-$ as a signal due to the moving spins plus additive random noise, we obtain

$$\begin{aligned} \mathbf{S}_{\mathrm{CD}} = |&2A\,\sin(\Delta\phi)e^{i(\phi_0+\pi/2)} + (\mathbf{n}_{r_+} - \mathbf{n}_{r_-}) \\ &+ i(\mathbf{n}_{i_+} - \mathbf{n}_{i_-})|, \end{aligned} \tag{5}$$

where $(\mathbf{n}_{r+} - \mathbf{n}_{r-})$ and $(\mathbf{n}_{i+} - \mathbf{n}_{i-})$ are independent zero-mean Gaussian random variables of equal variance $2\sigma_n^2$. This is a situation of order $N=2$ for which the two independent noise contributions reside in the separate quadrature components from real and imaginary channels of the complex dif-

ference. Without loss of generality, we can drop the complex exponential factor $\exp[i(\phi_0+\pi/2)]$; this step merely represents a rotation of phasors about the origin in the complex plane and will not affect the statistical properties of the resulting modulus image. In regions of no flow ($\Delta\phi=0$) as well as in the air background ($A=0$), the magnitude image of the residual complex noise as calculated by Eq. (4) will have a Rayleigh distribution. It is important to notice that the complex difference calculation is an envelope detection method yielding only magnitude information. The phase difference calculation, on the other hand, is an inherently coherent method that is also providing directional flow information. Noll *et al.*[23] provide an excellent treatise covering the effect of noise on SNR and contrast in coherent versus envelope detection for standard MR images. While the focus of that paper was on standard and inversion-recovery MR images, the analysis is equally valid for phase contrast imaging with encoding of flow in a single direction.

C. Flow encoding in multiple orthogonal directions

When flow is encoded in more than one physical direction, the calculations of Eqs. (2) and (4) must be carried out separately for each direction and combined to form a vector magnitude measuring total flow velocity. Directional information from the phase difference calculations is hereby disregarded, although it remains available in the individual sets of data, as discussed above. For flow encoding in all three orthogonal Cartesian coordinate directions using a six-point method, we obtain the processed phase contrast image magnitude as the norm,

$$\|\mathbf{S}_{\mathrm{PD}}\| = \sqrt{\mathbf{S}_{x,\mathrm{PD}}^2+\mathbf{S}_{y,\mathrm{PD}}^2+\mathbf{S}_{z,\mathrm{PD}}^2} \tag{6}$$

or

$$\|\mathbf{S}_{\mathrm{CD}}\| = \sqrt{\mathbf{S}_{x,\mathrm{CD}}^2+\mathbf{S}_{y,\mathrm{CD}}^2+\mathbf{S}_{z,\mathrm{CD}}^2}. \tag{7}$$

From Eqs. (3) and (5) it becomes evident that $\|\mathbf{S}_{\mathrm{PD}}\|$ and $\|\mathbf{S}_{\mathrm{CD}}\|$ are the norms of vectors in signal spaces of dimensions $N=3$ and $N=6$, respectively. That is, for phase difference processing, the dimension or number of degrees of freedom N directly equals the number of orthogonal Cartesian directions in which flow is encoded. For complex difference processing, the dimension N of the signal space is twice the physical dimension.

III. STATISTICAL DESCRIPTION

Let $\mathbf{s}_1,\ldots,\mathbf{s}_N$ be N independent jointly Gaussian random variables of equal variance σ^2 but possibly different mean m_i. The joint probability density function will have the following form:

$$f_{\mathbf{s}_1\cdots\mathbf{s}_N}(s_1,\ldots,s_N) = \frac{1}{(\sqrt{2\pi\sigma^2})^N}\exp[-\Sigma_{i=1}^N(s_i-m_i)^2/2\sigma^2]. \tag{8}$$

We have adopted the standard convention where boldface $\mathbf{s}_i$ denotes the random variable while s_i is used as place holder for a value of that random variable. The vector or N-tuple $(s_1,\ldots,s_N)$ can be interpreted as an element in a Hilbert space of dimension N. In the context of phase contrast image processing, the vector coordinates $\mathbf{s}_i$ represent either real values from phase difference calculations (e.g., $m_1=2A\Delta\phi$ and $\sigma_1^2=2\sigma_n^2$) or real and imaginary values from complex difference calculations before the modulus operation [e.g., $m_1=2A\sin(\Delta\phi)$, $m_2=0$, and $\sigma^2=\sigma_1^2=\sigma_2^2=2\sigma_n^2$].

In the following, we will derive a complete statistical description for the vector magnitude (norm) in terms of its associated probability density function for any number of degrees of freedom N. This will be the probability density function that fully characterizes the statistical properties of the processed phase contrast image magnitude obtained as $\|\mathbf{S}_{\mathrm{PD}}\|$ or $\|\mathbf{S}_{\mathrm{CD}}\|$ according to Eqs. (6) and (7), respectively. The vector magnitude of the N jointly Gaussian random variables $\mathbf{s}_i$ is calculated from

$$\mathbf{m} = \sqrt{\sum_{i=1}^N \mathbf{s}_i^2}. \tag{9}$$

We will be using M to denote the vector magnitude of the means of the individual random variables so that

$$M = \sqrt{\sum_{i=1}^N m_i^2}. \tag{10}$$

Here, M represents the deterministic signal component contribution to the observed vector magnitude m. Note that only the size of M is relevant. Since the random variables $\mathbf{s}_i$ are mutually uncorrelated and of equal variance, the direction of the vector $(m_1,\ldots,m_N)$ is immaterial; e.g., for two degrees of freedom in the case of complex difference processing mentioned above, we can consider $m_2=0$. The functional form of the probability density $f_{\mathbf{m}}(m)$ for the vector magnitude is preserved under any coordinate rotation in N-dimensional signal space.

It is important to realize the distinction between M and the mean of the random variable $\mathbf{m}$, i.e., the norm of the mean and the mean of the norm. Only when $M\gg\sigma$, as encountered in a fast-flow scenario, do we have a situation in which $M\approx E\{\mathbf{m}\}$, where $E\{\cdot\}$ denotes the statistical expectation. In that case we find that the dimension of the problem is reduced to unity and the vector magnitude becomes Gaussian with mean M and variance σ_2 regardless of the number of directions of flow encoding and type of phase contrast image processing employed,

$$f_{\mathbf{m}}(m) = \frac{1}{\sqrt{2\pi\sigma^2}}e^{-(m-M)^2/2\sigma^2}. \tag{11}$$

Indeed, in the limit as the signal component M becomes large compared to the standard deviation σ of the noise in each individual channel, the following expressions derived for the density $f_{\mathbf{m}}(m)$ will all approach this Gaussian form. The difference lies in the degree to which $f_{\mathbf{m}}(m)$ approximates a Gaussian for a particular value of M. The overall trend is that for a higher number of degrees of freedom N, a larger value of M is required in order that the probability

density function $f_{\mathbf{m}}(m)$ be reasonably Gaussian. Stated differently, the nonlinear threshold effect sets in at higher signal levels the higher the dimension N.

A. Single Gaussian random variable (one dimension)

Consider the observation "vector" magnitude,

$$\mathbf{m}=\sqrt{\mathbf{s}_1^2}=|\mathbf{s}_1|, \tag{12}$$

where $\mathbf{s}_1$ is Gaussian with variance σ^2 and mean M. Since $\mathbf{m}$ is simply the magnitude of the observation $\mathbf{s}_1$, the associated probability density function $f_{\mathbf{m}}(m)$ can be determined from

$$f_{\mathbf{m}}(m)=[f_{\mathbf{s}_1}(m)+f_{\mathbf{s}_1}(-m)]u(m) \tag{13}$$

or

$$f_{\mathbf{m}}(m)=\begin{cases}\dfrac{2}{\sigma\sqrt{2\pi}}\,e^{-(m^2+M^2)/2\sigma^2}\cosh\left(\dfrac{mM}{\sigma^2}\right)u(m), & \text{for } M>0,\\[2ex] \dfrac{2}{\sigma\sqrt{2\pi}}\,e^{-m^2/2\sigma^2}u(m), & \text{for } M=0.\end{cases} \tag{14}$$

The unit step function $u(m)$ is being used to indicate that the expression for the density $f_{\mathbf{m}}(m)$ is valid for non-negative values of the magnitude m only.

B. Jointly Gaussian random variables in two dimensions

Consider the observation vector magnitude,

$$\mathbf{m}=\sqrt{\mathbf{s}_1^2+\mathbf{s}_2^2}, \tag{15}$$

where $\mathbf{s}_1$ and $\mathbf{s}_2$ are jointly Gaussian with equal variance σ^2 and M is the vector magnitude of the means of $\mathbf{s}_1$ and $\mathbf{s}_2$. Following a transformation from rectangular coordinates (s_1,s_2) to polar coordinates (m,θ) and integration over the angle θ, the familiar Rician density for the magnitude $\mathbf{m}$ is readily obtained,[19,27]

$$f_{\mathbf{m}}(m)=\begin{cases}\dfrac{m}{\sigma^2}\,e^{-(m^2+M^2)/2\sigma^2}I_0\left(\dfrac{mM}{\sigma^2}\right)u(m), & \text{for } M>0,\\[2ex] \dfrac{m}{\sigma^2}\,e^{-m^2/2\sigma^2}u(m), & \text{for } M=0.\end{cases} \tag{16}$$

$I_0(\cdot)$ is the modified Bessel function of order zero. For $M=0$ in the absence of any signal component, the vector magnitude follows a Rayleigh distribution.

C. Jointly Gaussian random variables in three dimensions

Now, let $\mathbf{s}_1$, $\mathbf{s}_2$, and $\mathbf{s}_3$ be independent Gaussian random variables, each having a variance of σ^2. Let the means of $\mathbf{s}_1$ and $\mathbf{s}_2$ be zero while $\mathbf{s}_3$ is assumed to have a mean of M. The joint density of $\mathbf{s}_1$, $\mathbf{s}_2$, and $\mathbf{s}_3$ has the following form:

$$f_{\mathbf{s}_1\mathbf{s}_2\mathbf{s}_3}(s_1,s_2,s_3)=\frac{1}{(\sqrt{2\pi\sigma^2})^3}\,e^{[s_1^2+s_2^2+(s_3-M)^2]/2\sigma^2}. \tag{17}$$

When we consider the magnitude $\mathbf{m}$ where $\mathbf{m}=\sqrt{\mathbf{s}_1^2+\mathbf{s}_2^2+\mathbf{s}_3^2}$, its associated probability density function can be determined from the relationship

$$\begin{aligned}f_{\mathbf{m}}(m)\,dm&=\Pr\{m<\sqrt{\mathbf{s}_1^2+\mathbf{s}_2^2+\mathbf{s}_3^2}\leq m+dm\}\\&=\int\int\int_{\Delta D_m} f_{\mathbf{s}_1\mathbf{s}_2\mathbf{s}_3}(s_1,s_2,s_3)\,ds_1\,ds_2\,ds_3,\end{aligned} \tag{18}$$

where ΔD_m is a spherical shell in the (s_1,s_2,s_3)-coordinate system with inner radius m and thickness dm, and $\Pr\{\cdot\}$ denotes probability. By introducing a transformation from rectangular coordinates (s_1,s_2,s_3) to spherical coordinates (m,θ,ϕ) and integrating with respect to the volume element $ds_1\,ds_2\,ds_3=m^2\,dm\,d\theta\sin\phi\,d\phi$, the probability density function of the vector magnitude can then be expressed as

$$f_{\mathbf{m}}(m)=\begin{cases}\dfrac{2}{\sigma\sqrt{2\pi}}\,\dfrac{m}{M}\,e^{-(m^2+M^2)/2\sigma^2}\sinh\left(\dfrac{mM}{\sigma^2}\right)u(m), & \text{for } M>0,\\[2ex] \dfrac{2m^2}{\sigma^3\sqrt{2\pi}}\,e^{-m^2/2\sigma^2}u(m), & \text{for } M=0.\end{cases} \tag{19}$$

This is an extension of the prior result for the Rician distribution with two degrees of freedom to the case of jointly Gaussian random variables in three dimensions. For $M=0$ in the absence of any signal component, the vector magnitude has a Maxwell probability density.

D. Generalization of the density of magnitude for any order

The approach of using a transformation from rectangular to polar coordinates becomes very tedious for higher order N. For jointly Gaussian random variables of equal variance in a hyperspace of dimension N, a general form of the expression for the density of the vector magnitude can be found by first considering the square of the magnitude,

$$\mathbf{y}=\mathbf{m}^2=\sum_{i=1}^{N}\mathbf{s}_i^2. \tag{20}$$

The random variables $\mathbf{s}_i$ are independent Gaussian of equal variance σ^2 but possibly different mean m_i. Again, let M denote the vector magnitude of the means of the individual $\mathbf{s}_i$. By deriving the characteristic function of the random variable $\mathbf{y}$ and subsequently invoking Laplace transform relationships for the modified Bessel function, we can determine as shown in Appendix A that the resulting probability density function $f_{\mathbf{y}}(y)$ of $\mathbf{y}$ for arbitrary N becomes of a form:

$$f_{\mathbf{y}}(y)=\frac{1}{2\sigma^2}\left(\frac{y}{M^2}\right)^{(N-2)/4}e^{-(y+M^2)/2\sigma^2}I_{N/2-1}\left(\frac{\sqrt{y}M}{\sigma^2}\right)u(y). \tag{21}$$

Next, consider a transformation from the intermediate random variable $\mathbf{y}$ to the desired random variable $\mathbf{m}$ where $\mathbf{m}=\sqrt{\mathbf{y}}$, as implied by Eq. (20). The resulting probability density function for $\mathbf{m}$ can then be expressed in terms of the density for $\mathbf{y}$ as

$$f_{\mathbf{m}}(m)=2mf_{\mathbf{y}}(m^2). \tag{22}$$

Substituting the expression for $f_{\mathbf{y}}(y)$ from above, we obtain the desired density of the observation vector magnitude $\mathbf{m}$ in a hyperspace of arbitrary dimension N,

$$f_{\mathbf{m}}(m)=\frac{m^{N/2}}{\sigma^2M^{N/2-1}}e^{-(m^2+M^2)/2\sigma^2}I_{N/2-1}\left(\frac{mM}{\sigma^2}\right)u(m),\quad \text{for}\quad M>0. \tag{23}$$

When we also consider Bessel functions of noninteger order, the expression for the probability density function can be evaluated for a hyperspace of any dimension, odd or even. In particular, Sommerfeld's notation can be used to write the half-order modified spherical Bessel functions as[28]

$$\sqrt{\frac{\pi}{2z}}I_{-1/2}(z)=\frac{\cosh z}{z} \tag{24}$$

and

$$\sqrt{\frac{\pi}{2z}}I_{1/2}(z)=\frac{\sinh z}{z}, \tag{25}$$

leading to the specific expressions of Eqs. (14) and (19) for $f_{\mathbf{m}}(m)$ in signal spaces of order $N=1$ and $N=3$, respectively.

In the limit as the signal component amplitude approaches zero, $M\to 0$, the expression for the probability density function of the vector magnitude will approach that of the familiar χ distribution of order N,[27]

$$f_{\mathbf{m}}(m)=\frac{2m^{N-1}}{(\sigma\sqrt{2})^N\Gamma(N/2)}e^{-m^2/2\sigma^2}u(m),\quad \text{for}\quad M=0, \tag{26}$$

where $\Gamma(\cdot)$ is the Gamma function. This is the distribution of the processed phase contrast image voxel in the absence of any signal component due to flow. The Rayleigh and Maxwell distributions referred to above are special cases of the general χ distribution for order $N=2$ and $N=3$. For $M>0$, we may say that the random variable $\mathbf{m}$ has a noncentral χ distribution.

In the other limit as $M\to\infty$, we can use the asymptotic form $I_\nu(z)\sim e^z/\sqrt{2\pi z}$ of the modified Bessel function for large argument z to show that the density $f_{\mathbf{m}}(m)$ is Gaussian in the form of Eq. (11) for values $m\approx M$. Since in this limit $M\gg\sigma$, the exponential form of the Gaussian drops off much faster on either side of M compared to the variation in the ratio $(m/M)^{(N-1)/2}$ left as a factor from substitution of the asymptotic form, and the Gaussian expression becomes valid for all m and N. That is, for large M, only the noise component aligned with the deterministic (signal) component phasor will be of any significance. Qualitatively, this result can be readily supported by the generalization to N-dimensional signal space of a simple vector graphics argument using phasors as well.[26]

E. Statistical averages

The statistical averages of mean and variance are determined from the integrals defining first- and second-order moments,

$$E\{\mathbf{m}\}=\int_{-\infty}^{\infty}mf_{\mathbf{m}}(m)dm, \tag{27}$$

$$E\{\mathbf{m}^2\}=\int_{-\infty}^{\infty}m^2f_{\mathbf{m}}(m)dm, \tag{28}$$

and

$$\mathrm{Var}\{\mathbf{m}\}=E\{\mathbf{m}^2\}-[E\{\mathbf{m}\}]^2. \tag{29}$$

The mean-squared or total error in turn is defined commonly as

$$E\{[\mathbf{m}-M]^2\}=E^2\{\mathbf{m}-M\}+\mathrm{Var}\{\mathbf{m}\}, \tag{30}$$

where $E\{\mathbf{m}-M\}$ is the bias incurred when we use the observation magnitude m to estimate the underlying signal component M. Substituting the specific form for the probability density function $f_{\mathbf{m}}$ of the vector magnitude $\mathbf{m}$ given in Eq. (23), we must evaluate an integral of the form

$$E\{\mathbf{m}\}=\int_0^\infty \frac{m^{N/2+1}}{\sigma^2 M^{N/2-1}} e^{-(m^2+M^2)/2\sigma^2} I_{N/2-1}\left(\frac{mM}{\sigma^2}\right) dm$$

$$=\frac{e^{-M^2/2\sigma^2}}{\sigma^2 M^{N/2-1}} \int_0^\infty m^{N/2+1} e^{-m^2/2\sigma^2} I_{N/2-1}\left(\frac{mM}{\sigma^2}\right) dm. \tag{31}$$

From Mellin transform tables,[29] the following relationship for the integral is obtained:

$$\int_0^\infty x^{s-1} e^{-\beta^2 x^2} I_\nu(\alpha x) dx = \frac{i^{-\nu-1}\Gamma[(\nu+s)/2] e^{\alpha^2/8\beta^2}}{\alpha\beta^{s-1}\Gamma(\nu+1)} \times M_{(s-1)/2,\nu/2}\left(-\frac{\alpha^2}{4\beta^2}\right), \tag{32}$$

where $M_{\mu,\kappa}(\cdot)$ is the Whittaker function. Subsequently, the Whittaker function $M_{\mu,\kappa}(z)$ can be expressed in terms of confluent hypergeometric functions $\Phi(\frac{1}{2}-\kappa+\mu,2\mu+1;z)$ as

$$M_{(s-1)/2,\nu/2}(z)=e^{-(1/2)z} z^{(\nu+1)/2} \Phi\left(1+\frac{\nu-s}{2},1+\nu;z\right). \tag{33}$$

Substituting Eqs. (32) and (33) into Eq. (31), we find the mean as

$$E\{\mathbf{m}\}=\sqrt{2}\sigma \frac{\Gamma[(N+1)/2]}{\Gamma(N/2)} \Phi\left(-\frac{1}{2},\frac{N}{2};-\frac{M^2}{2\sigma^2}\right),$$
$$E\{\mathbf{m}|0\}=\sqrt{2}\sigma \frac{\Gamma[(N+1)/2]}{\Gamma(N/2)}, \quad \text{for } M=0. \tag{34}$$

When recurrence relations between confluent hypergeometric functions of different values for the indices are used, the needed function for specific values of the order N can be expressed in terms of special cases for which the confluent hypergeometric functions become modified Bessel, Laguerre, and error functions (see Appendix B).

Recalling that $\mathbf{m}^2$ has a noncentral χ^2 distribution with N degrees of freedom, the mean of the square can be written as $E\{\mathbf{m}^2\}=N\sigma^2+M^2$. In turn, the variance of the random variable $\mathbf{m}$ representing the observation vector magnitude can be expressed in terms of the mean $E\{\mathbf{m}\}$ as

$$\text{Var}\{\mathbf{m}\}=N\sigma^2+M^2-[E\{\mathbf{m}\}]^2. \tag{35}$$

From asymptotic expansions of error and Bessel functions for large argument,[30] it follows that

$$E\{\mathbf{m}\}-M\to 0, \quad \text{as } M\to\infty \tag{36}$$

and

$$\text{Var}\{\mathbf{m}\}\to\sigma^2, \quad \text{as } M\to\infty, \tag{37}$$

regardless of the order N. That is, for large M, only the noise component aligned with the deterministic (signal) component will be of any significance, thus leading to a Gaussian probability density function in the form of Eq. (11). We note here that, while $E\{\mathbf{m}\}\to M$ in the limit as $M\to\infty$, it follows directly from asymptotic expansions that $[E\{\mathbf{m}\}]^2\to M^2+(N-1)\sigma^2$ as $M\to\infty$. Therefore, we find, as indicated in Eq. (37) above, that the variance $\text{Var}\{\mathbf{m}\}\to\sigma^2$ as $M\to\infty$ rather than $\text{Var}\{\mathbf{m}\}\to N\sigma^2$, as one might otherwise have suspected in the limit as $M\to\infty$.

IV. RESULTS AND DISCUSSION

Figures 1(a) and 1(b) illustrated the probability density functions $f_{\mathbf{m}}(m)$ associated with the observed vector magnitude $\mathbf{m}$ for values $M=0$ and $M=5$ of the underlying signal component magnitude, respectively. The case of $M=0$ represents background noise only, i.e., $A/\sigma_n \gg 1$ within an object in the image but $\Delta\phi=0$ since no flow is present. Plots are shown for orders $N=1$, $N=2$, $N=3$, and $N=6$ with a value of $\sigma^2=2$ chosen for the variance. Since $\sigma^2=2\sigma_n^2$ denotes the variance of the independent noise contributions in difference images calculated according to Eqs. (3) and (5), a value of $\sigma^2=2$ reflects a variance of $\sigma_n^2=1$ for the intrinsic noise in real and imaginary channels of the base images. Thus, we can think of the amplitudes and in turn the observed vector magnitude as being normalized with respect to the inherent image noise standard deviation σ_n, i.e., values along the abscissa represent the values of m/σ_n in general. Physically, orders $N=1$ and $N=3$ pertain to phase difference processing for encoding of flow in one and three orthogonal directions, respectively. Orders $N=2$ and $N=6$ are for complex difference processing. [Likewise, $f_{\mathbf{m}}(m)$ for $N=4$ could be shown; that case, however, corresponds to complex difference processing of base image data from the more uncommon scenario of flow encoding in two orthogonal directions.] The order N is shown to have much greater influence at $M=0$ as compared to $M=5$.

Experimental data for verification of the noise analysis have been collected using a cylindrical agar phantom as a plug flow model that yielded uniform velocity distributions under a controlled drive. Velocity encoding was varied from 130 to 10 cm/s to obtain the range of the desired phase information. Since the induced phase difference $2\Delta\phi \ll \pi$, we need not be concerned with wrapping of the phase nor with contributions from noise in the magnitude mask for phase difference processing. The inherent noise standard deviation σ_n was determined from ROI measurements in the air background of the base images. The signal component magnitude M was determined as the ROI sample mean in a coherently detected phase difference image and normalized with respect to the inherent noise standard deviation σ_n. Figure 1(c) is a histogram from pure noise for a ROI in the air background of a complex difference processed magnitude image calculated from a set of six independent base images (order $N=6$). Excellent correspondence is shown with the probability density function predicted by the theory (dashed line).

The density function $f_{\mathbf{m}}(m)$ of the observation vector magnitude can be interpreted as a conditional density function $f_{\mathbf{m}|M}(m|M)$, where a specific value of the signal component magnitude M represents the conditioning event. Plots of $f_{\mathbf{m}}(m)$ over a range of values for M then represent the joint density function $f_{\mathbf{m},\mathbf{M}}(m,M)$ for a uniformly distributed flow signal magnitude M. Contour plots of the joint density are shown in Figs. 2(a)–2(d) for different values of the num-

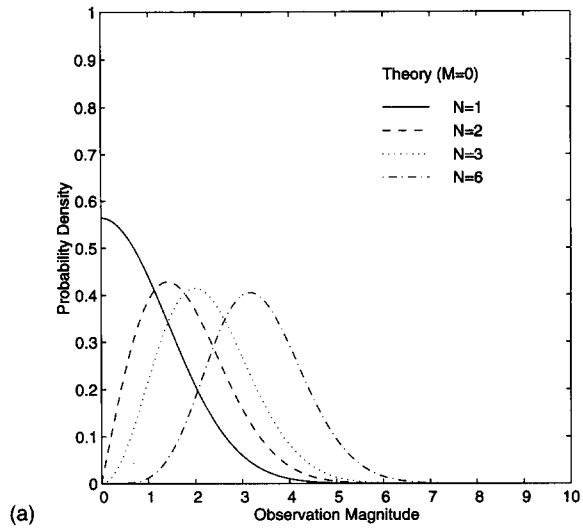

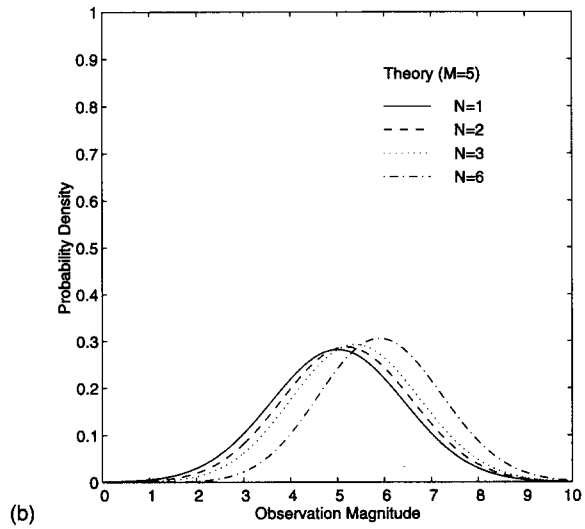

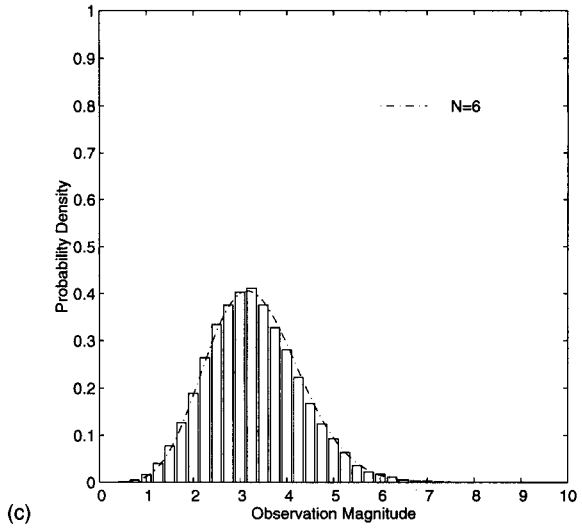

FIG. 1. Probability density functions of observation vector magnitude for (a) $M=0$ and (b) $M=5$; (c) histogram of experimental data, $M=0$.

ber of degrees of freedom N. For small values of the signal component associated with flow, $M/\sigma_n<2$, we notice a shift of the density function toward comparably larger values of the observation magnitude. This shift is consistent with the bias $E\{\mathbf{m}-M\}$ being larger for small M, where the observation vector magnitude m is dominated by the contributions from independent noise components. As one would expect, the amount of bias is also shown to increase with an increase in the number of degrees of freedom N in the flow experiment.

By evaluating Eq. (34) for specific values of the order N, as given by Eqs. (B1), (B2), (B3), and (B5) in Appendix B over a range of values for the signal component magnitude M, plots of the observed vector mean $E\{\mathbf{m}\}$ can be obtained, as shown in Fig. 3. For the previously studied special case of $N=2$, Henkelman[21] has calculated the mean of conventional magnitude MR images by direct integration. In their comparison of phase-corrected real and magnitude reconstructed MR images, Bernstein *et al.*[22] stated the closed-form expression for the mean originally derived by Rice.[37] In general, when values for the mean are substituted into Eq. (35), the variance in turn can be found as a function of M. From the plots shown in Fig. 4, we see that for large signal M, the variance approaches a value of 2 (i.e., $2\sigma_n^2$) regardless of the number of degrees of freedom N. An interesting observation is the crossover of the variance curves at about $M\approx 1$. It is misleading to interpret the lower value for the variance at small values of the signal component M as somehow facilitating the detection of slow flow. From Fig. 3 it follows that the mean $E\{\mathbf{m}\}$ remains largely unaffected by changes in signal over a range $M/\sigma_n<2$. Likewise, we see from the contour plots in Fig. 2 that the shape of the density function $f_{\mathbf{m}}(m)$ stays virtually the same for such small M. Stated differently, observations on the level end of the (joint) probability density contain only very little information about the underlying signal component magnitude. The experimental data shown in Figs. 3 and 4 were determined from sample analysis of 500 pixels in ROIs collected from a region of the calculated phase contrast magnitude images containing the agar phantom. Since the variance is a second-order statistical property and therefore is affected by any inaccuracy in the estimate of the mean or by a "profiling" inhomogeneity in

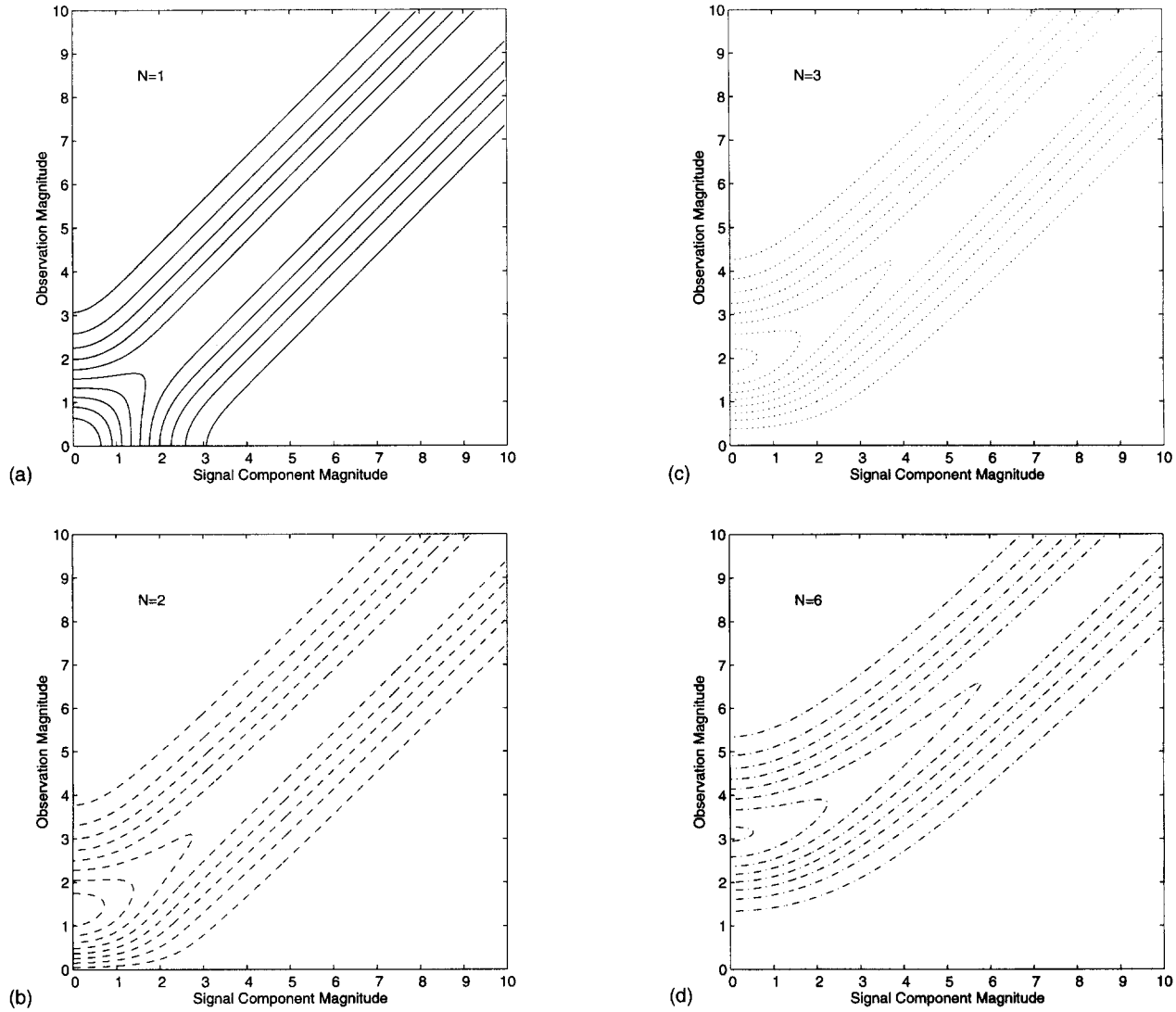

FIG. 2. Joint probability density functions of observation vector and signal component magnitudes for order (a) $N=1$, (b) $N=2$, (c) $N=3$, and (d) $N=6$.

the reconstructed image, the estimates of variance are less accurate than are estimates of the mean.

In a quantitative analysis of flow in phase contrast images, the bias represents an error in the reconstructed pixel magnitude values. For the Rician distribution of image magnitude (order $N=2$), methods have been proposed for a reduction of the bias in $E\{\mathbf{m}^2\}$ and $E\{\mathbf{m}\}$, respectively.[32,33] This kind of an approach may have some appeal in the ROI analysis of a large homogeneous region within an image, where calculated sample mean and variance values are used in lieu of statistical ensemble averages over repeated measurements. Yet, since the bias of a magnitude image taken in the strict sense of the statistical mean for that pixel position is not merely an additive component, it cannot just simply be subtracted out. In phase contrast image processing, an estimate must be calculated on a pixel-by-pixel basis from a single observation value, and knowledge of the actual shape and skewness of the probability distribution becomes essential. On the other hand, when $M=0$ in the absence of any signal component pertaining to flow, the mean $E\{\mathbf{m}|0\}$ represents

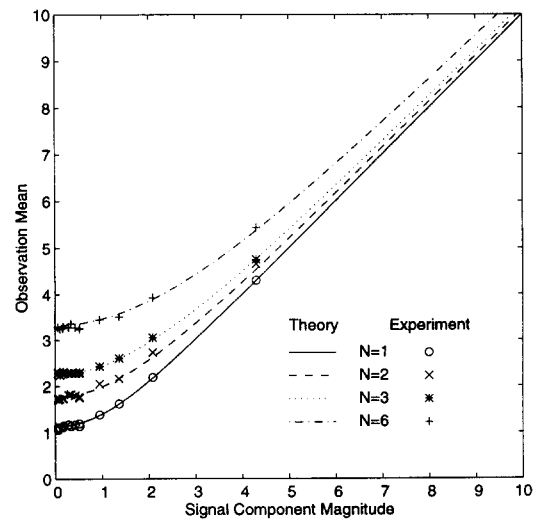

FIG. 3. Illustrating the dependence of the mean of the observation vector magnitude on the signal component magnitude. (Experimental data was shown at the 1993, 12th annual meeting of the SMRM.[31])

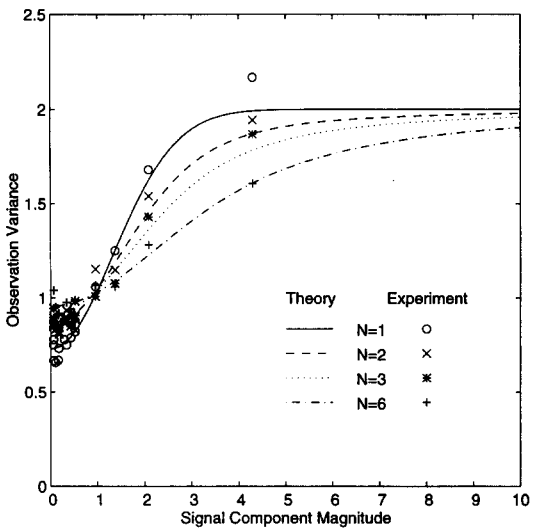

FIG. 4. Illustrating the dependence of the variance of the observation vector magnitude on the signal component magnitude.

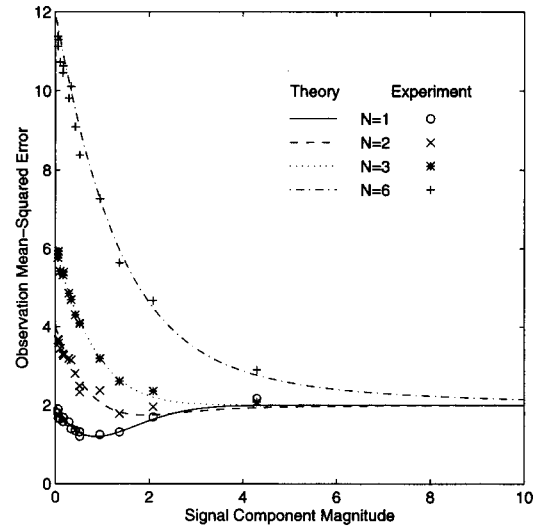

FIG. 5. Illustrating the dependence of the mean-squared error on the signal component magnitude.

the background noise level within an object in the processed phase contrast image. The flat part at low M in plots of the joint density as well as of the mean therefore is indicative of a nonlinear threshold effect. Hence, in order that a vessel may be detected in a phase contrast image, its signal level associated with flow must exceed a certain threshold. It appears that this threshold increases with an increase in the number of degrees of freedom in the flow experiment. The commonly used MIP (maximum intensity projection) technique for visualizing vessel structures from a volume of multiple partitions in MR angiography is known to reduce the vessel contrast.[34] The bias in individual partition images due to noise at slow flow rates or in the absence of flow will be significantly elevated in a MIP image from many such partitions and to varying degree depending again on the number of degrees of freedom in the flow experiment. The quantitative assessment of the problem of detection and estimation is an ongoing effort.

When the observed vector magnitude $\mathbf{m}$ is being used in quantitative analysis as an estimate of the underlying flow-related signal component magnitude M, the total or mean-squared error is a more meaningful measure of fidelity. The mean-squared error combines the effects of bias and variance errors. Figure 5 illustrates plots of the mean-squared error for specific values of the order N. The dip in the curve for $N=1$ is caused by the bias contribution to the mean-squared error decreasing initially at a faster rate than the accompanying increase in the variance contribution for an increase in the signal component M.

Also, the signal-to-noise ratio is a commonly used measure of image quality combining mean and standard deviation as a function of M:[23]

$$\mathrm{SNR}_{\mathrm{OUT}}=\frac{E\{\mathbf{m}|M\}-E\{\mathbf{m}|0\}}{\sqrt{\mathrm{Var}\{\mathbf{m}|M\}}}. \tag{38}$$

It should be noted that the definition of the SNR is based on statistical expected values for individual pixel locations, considered across an ensemble of images from repeated observations. Figure 6 illustrates the dependence of the resulting output signal-to-noise ratio of processed phase contrast images on the underlying flow signal component amplitude M. We refer to the signal-to-noise ratio for coherent detection in the direction of flow as the "input" $\mathrm{SNR}_{\mathrm{IN}}=M/\sigma$. The departure from a linear curve representing coherent detection is due to a lack of *a priori* information about the actual direction of flow and to the use of a vector magnitude (envelope) calculation. For input $\mathrm{SNR}_{\mathrm{IN}}=3$ dB or $M/\sigma=1.414$, the output signal-to-noise ratio is about 2 dB higher for $N=3$ than for $N=6$. That is, the $\mathrm{SNR}_{\mathrm{OUT}}$ for phase difference process-

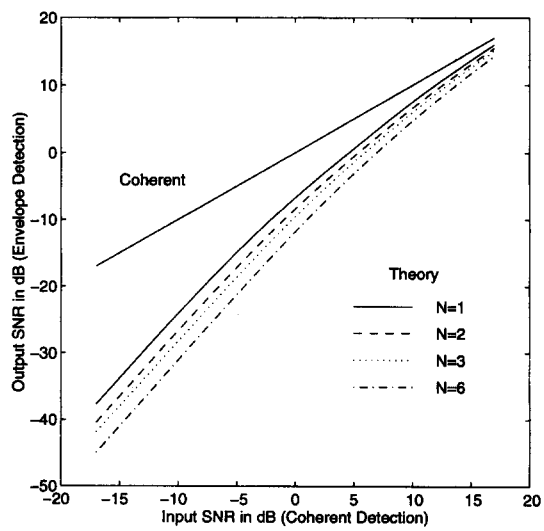

FIG. 6. Illustrating the observation vector magnitude signal-to-noise ratio as a function of the inherent signal-to-noise ratio for coherent detection.

ing is 25% superior to that for complex difference processing when flow is encoded in all three orthogonal Cartesian directions.

Partial voluming from stationary and moving spins within the same voxel has been shown to affect the signal component differently, depending on the method of phase contrast image processing being used, complex difference, or phase difference.[2] Since the noise contributions are uncorrelated to the signal and thus remain unaffected, the results presented here are applicable in this situation as well. One must enter an appropriate value of M that reflects the altered phase contrast signal amplitude due to the presence of static spins within the voxel. The commonly low amplitude found in the processed difference image signal when partial volume effects and/or slow flow are present emphasizes the importance in the analysis of the interaction of signal and noise presented in this paper.

The frequently used four-point method is based on a common flow-compensated acquisition for the three orthogonal directions of flow encoding.[8] Since this scheme leads to noise contributions that are correlated between the three Cartesian directions, the interaction of signal and random noise cannot be described statistically using the model developed here. However, sample mean and variance can be readily determined from computer generated realizations of Gaussian random noise processes. Plots of the sample mean and variance for increasing value of the signal component magnitude M are shown in Figs. 7 and 8, respectively. From Fig. 7 we see that the means of the observation vector magnitude $\mathbf{m}$ for phase difference as well as complex difference processing from a simulated four-point acquisition closely follow those for a six-point method, where noise is independent among the three directions of flow encoding (order $N=3$ and $N=6$, respectively). The variance, on the other hand, is considerably higher in the case of correlated noise, as encountered with the four-point method. We must stress, however, that these are estimates only; we do not know the underlying probability density function. A histogram analysis would show an initial faster rise coupled with a prolonged tail as compared to the corresponding scenarios of independent noise for the six-point method shown in Fig. 1. Thus, we find an approximately equal mean but a higher variance. Without knowledge of the probability density function, we will not be able to subsequently characterize the effect of noise on calculated MIP images, nor can we develop signal processing methods for statistically optimal detection and estimation.

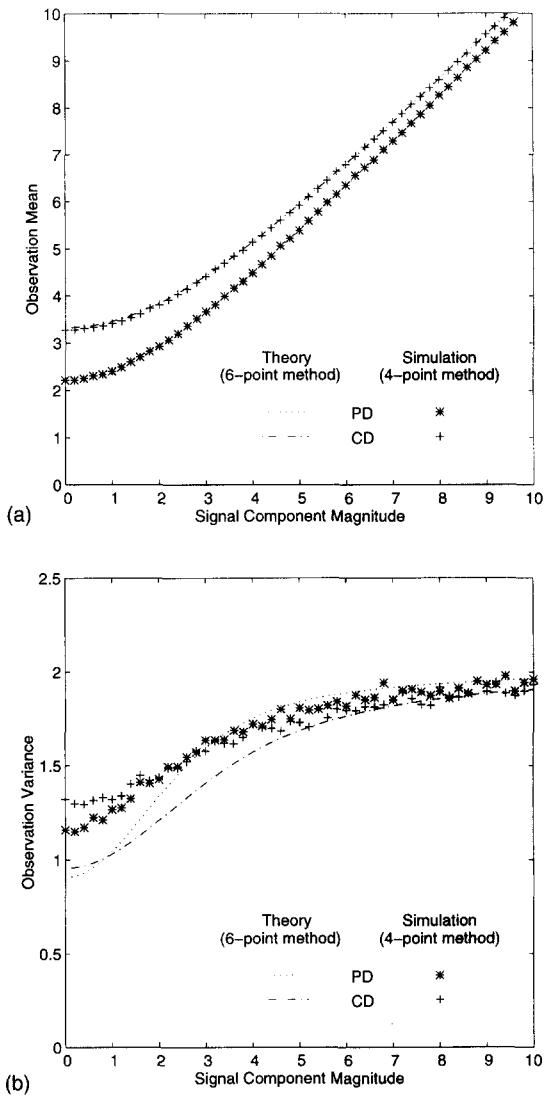

FIG. 7. Computer simulations of the four-point method illustrating the dependence of (a) the sample mean and (b) the sample variance of the observation vector on the signal component magnitude. Estimates for phase difference (PD) and for complex difference (CD) processing are shown along with the corresponding theoretical values for the six-point method.

V. CONCLUSION

The statistical properties of the phase contrast image vector magnitude at slow flow rates are strongly affected by the number of degrees of freedom in the flow experiment. This is evidenced by the nonlinear behavior of the mean, variance, and signal-to-noise ratio. A complete statistical description has been presented that is valid at all rates of flow for any number of independent flow encoding directions and type of phase contrast image processing. The results leading to the general form of Eq. (23) for the probability density function and Eq. (34) for the mean of the phase contrast image magnitude are novel.

Results show a progressively increased bias in the processed phase contrast image magnitude at slow flow rates due to contributions from inherent random noise. The amount of this bias increases with the number of physical directions in which flow is encoded and is noticeably larger for complex difference processed images than for phase difference processing. Correspondingly, the phase contrast image signal-to-noise ratio associated with flow as well as the vessel contrast become compromised. In comparing the results for encoding of slow flow in all three directions, we have found that the signal-to-noise ratio for phase difference processing is about 25% superior to that for complex difference processing.

The knowledge provided by the statistical description de-

veloped here will make possible the subsequent characterization of the properties of signal and noise in MIP images from multiple slices or partitions in a 3-D phase contrast image dataset. Likewise, we may engage in further work to develop the receiver operating characteristic, giving the performance of the phase contrast image processor as a receiver, and possibly derive an optimal Bayes estimator of the underlying signal component associated with flow.

ACKNOWLEDGMENTS

This work was supported in part by a grant from Siemens Medical Systems and in part by the Center for Magnetic Resonance Imaging and Spectroscopy (MRISC) at the University of Kentucky. The authors thank S. Guarnieri for assistance with the design of the plug flow phantom.

APPENDIX A: PROBABILITY DENSITY OF THE SQUARED MAGNITUDE

As a first step in deriving the probability density function for the random variable $\mathbf{y}$ defined by Eq. (20), let $\mathbf{y}_1=\mathbf{s}_1^2$, where $\mathbf{s}_1$ is Gaussian with mean m_1 and variance σ^2. We find the associated characteristic function representing the Fourier transform of the probability density function as a statistical expectation,[27]

$$\begin{aligned}\Phi_{\mathbf{y}_1}(\omega)&=E\{e^{i\omega\mathbf{s}_1^2}\}\\&=\int_{-\infty}^{\infty}\frac{e^{i\omega s_1^2}}{\sqrt{2\pi\sigma^2}}e^{-(s_1-m_1)^2/2\sigma^2}\,ds_1\\&=\frac{e^{-m_1^2/2\sigma^2}}{\sqrt{2\pi\sigma^2}}\int_{-\infty}^{\infty}e^{-(1/2\sigma^2-i\omega)s_1^2}e^{(m_1/\sigma^2)s_1}\,ds_1.\end{aligned}\tag{A1}$$

With the exception of the proper normalization factor, the integral is the two-sided Laplace transform of a Gaussian function with complex "variance,"

$$\frac{1}{2(1/2\sigma^2-i\omega)},$$

evaluated at $s_1=m_1/\sigma^2$:

$$\begin{aligned}\Phi_{\mathbf{y}_1}(\omega)&=\frac{e^{-m_1^2/2\sigma^2}}{\sigma\sqrt{2(1/2\sigma^2-i\omega)}}\exp\left(\frac{(m_1/\sigma^2)^2}{4(1/2\sigma^2-i\omega)}\right)\\&=\frac{e^{-m_1^2/2\sigma^2}}{\sqrt{1-2i\omega\sigma^2}}\exp\left(\frac{m_1^2}{2\sigma^2(1-2i\omega\sigma^2)}\right)\\&=\frac{1}{\sqrt{1-2i\omega\sigma^2}}\exp\left(\frac{i\omega m_1^2}{(1-2i\omega\sigma^2)}\right).\end{aligned}\tag{A2}$$

Now consider the sum of the squares,

$$\mathbf{y}=\sum_{i=1}^{N}\mathbf{y}_i=\sum_{i=1}^{N}\mathbf{s}_i^2.\tag{A3}$$

Since the individual $\mathbf{s}_i$ are statistically independent, the integration for the expectation in the characteristic function for $\mathbf{y}$ becomes separable so that

$$\begin{aligned}\Phi_{\mathbf{y}}(\omega)&=E\left\{\left\{\exp\left(i\omega\sum_{i=1}^{N}\mathbf{s}_i^2\right)\right\}\right\}\\&=\prod_{i=1}^{N}E\{\exp(i\omega\mathbf{s}_i^2)\}=\prod_{i=1}^{N}\Phi_{\mathbf{y}_i}(\omega)\\&=\frac{1}{(1-2i\omega\sigma^2)^{N/2}}\exp\left(i\omega\sum_{i=1}^{N}m_i^2\Big/(1-2i\omega\sigma^2)\right)\\&=\frac{1}{(1-2i\omega\sigma^2)^{N/2}}\exp\left(\frac{i\omega M^2}{(1-2i\omega\sigma^2)}\right),\end{aligned}\tag{A4}$$

where we have introduced $M^2=\Sigma_{i=1}^{N}m_i^2$ as defined in Eq. (10). The probability density function $f_{\mathbf{y}}(y)$ in turn can be found as the inverse Fourier transform of its associated characteristic function $\Phi_{\mathbf{y}}(\omega)$ by

$$f_{\mathbf{y}}(y)=\frac{1}{2\pi}\int_{-\infty}^{\infty}\frac{1}{(1-2i\omega\sigma^2)^{N/2}}e^{i\omega M^2/(1-2i\omega\sigma^2)}e^{-i\omega y}\,d\omega.\tag{A5}$$

Now, if we let $s=1-2i\omega\sigma^2$, the Fourier transform relationship can be rewritten as an inverse Laplace transform,

$$\begin{aligned}f_{\mathbf{y}}(y)&=\frac{1}{2\sigma^2}\frac{1}{2\pi i}\int_{1-i\infty}^{1+i\infty}\frac{1}{s^{N/2}}e^{(1-s)(M^2/2\sigma^2)}\\&\quad\times e^{-(1-s)(y/2\sigma^2)}\,ds\\&=\frac{1}{2\sigma^2}e^{-(y+M^2)/2\sigma^2}\\&\quad\times\frac{1}{2\pi i}\int_{1-i\infty}^{1+i\infty}\frac{1}{s^{N/2}}e^{(m^2/2\sigma^2)/s}e^{s(y/2\sigma^2)}\,ds.\end{aligned}\tag{A6}$$

From Laplace transform tables,[35] we obtain

$$\frac{1}{s^{\mu}}e^{k/s}\Leftrightarrow\left(\frac{t}{k}\right)^{(\mu-1)/2}I_{\mu-1}(2\sqrt{kt}).\tag{A7}$$

With $\mu=N/2$ and $k=M^2/(2\sigma^2)$, we finally arrive at an expression for the probability density function of the intermediate random variable $\mathbf{y}$ valid for arbitrary order N,

$$f_{\mathbf{y}}(y)=\frac{1}{2\sigma^2}\left(\frac{y}{M^2}\right)^{(N-2)/4}e^{-(y+M^2)/2\sigma^2}I_{N/2-1}\left(\frac{\sqrt{y}M}{\sigma^2}\right)u(y),\tag{A8}$$

where $I_{N/2-1}(\cdot)$ is the modified Bessel function of order $N/2-1$. The random variable $\mathbf{y}$ representing the squared vector magnitude has what one may call a noncentral χ^2 distribution with N degrees of freedom. [For an inherently even order N, a similar form of the probability density in Eq. (A8) was first derived and used in evaluating the performance of incoherently terminated quadratic receivers in multichannel commu-

nication and radar detection systems (square-law detection for $N/2$ Rician bandpass channels with noise quadrature components).[24,25,36,37]]

APPENDIX B: EXPECTED VALUES FOR SPECIFIC DIMENSIONS N

For specific values of the order N, we can find closed-form expressions for mean and variance of the vector magnitude $\mathbf{m}$ in terms of familiar functions.

$N=1$: Substituting the probability density function of Eq. (14) into Eq. (27), integration for the mean readily leads to an expression in terms of exponential and error functions,

$$E\{\mathbf{m}\}=\sigma\left[\sqrt{\frac{2}{\pi}}\,e^{-M^2/2\sigma^2}+\frac{M}{\sigma}\,\mathrm{erf}\left(\frac{M}{\sqrt{2}\sigma}\right)\right],$$
$$E\{\mathbf{m}|0\}=\sqrt{\frac{2}{\pi}}\,\sigma. \tag{B1}$$

$N=2$:

$$E\{\mathbf{m}\}=\sqrt{\frac{\pi}{2}}\,\sigma e^{-M^2/4\sigma^2}\left[\left(1+\frac{M^2}{2\sigma^2}\right)I_0\left(\frac{M^2}{4\sigma^2}\right)+\frac{M^2}{2\sigma^2}\,I_1\left(\frac{M^2}{4\sigma^2}\right)\right], \tag{B2}$$
$$E\{\mathbf{m}|0\}=\sqrt{\frac{\pi}{2}}\,\sigma.$$

An expression for the mean of the Rician random variable can also be found in Papoulis,[27] Bernstein,[22] and Rice.[38]

$N=3$:

$$E\{\mathbf{m}\}=\sigma\left[\sqrt{\frac{2}{\pi}}\,e^{-M^2/2\sigma^2}+\left(\frac{\sigma}{M}+\frac{M}{\sigma}\right)\mathrm{erf}\left(\frac{M}{\sqrt{2}\sigma}\right)\right],$$
$$E\{\mathbf{m}|0\}=2\sqrt{\frac{2}{\pi}}\,\sigma. \tag{B3}$$

$N=4$:

$$E\{\mathbf{m}\}=\frac{3}{2}\sqrt{\frac{\pi}{2}}\,\sigma e^{-M^2/4\sigma^2}\left[\left(1+\frac{M^2}{3\sigma^2}\right)I_0\left(\frac{M^2}{4\sigma^2}\right)+\frac{1}{3}\left(1+\frac{M^2}{\sigma^2}\right)I_1\left(\frac{M^2}{4\sigma^2}\right)\right], \tag{B4}$$
$$E\{\mathbf{m}|0\}=\frac{3}{2}\sqrt{\frac{\pi}{2}}\,\sigma.$$

$N=6$:

$$E\{\mathbf{m}\}=\sqrt{2\pi}\,\sigma e^{-M^2/4\sigma^2}\left[\left(1+\frac{M^2}{4\sigma^2}\right)I_0\left(\frac{M^2}{4\sigma^2}\right)+\left(-\frac{\sigma^2}{2M^2}+\frac{1}{2}+\frac{M^2}{4\sigma^2}\right)I_1\left(\frac{M^2}{4\sigma^2}\right)\right], \tag{B5}$$
$$E\{\mathbf{m}|0\}=\frac{15}{8}\sqrt{\frac{\pi}{2}}\,\sigma.$$

[a]Address correspondence to: Anders H. Andersen, Ph.D., University of Kentucky Medical Center, 106 MRISC Bldg., 800 Rose Street, Lexington, Kentucky 40536-0098. Phone: (606) 323-1112; Fax: (606) 323-1068; Electronic mail: anders@mri.uky.edu.

[1]L. Axel and D. Morton, "MR flow imaging by velocity-compensated/uncompensated difference images," J. Comput. Assist. Tomogr. **11**, 31–34 (1987).

[2]M. A. Bernstein and Y. Ikezaki, "Comparison of phase- difference and complex-difference processing in phase-contrast MR angiography," J. Magn. Reson. Imag. **1**, 725–729 (1991).

[3]C. L. Dumoulin, S. P. Souza, M. F. Walker, and W. Wagle, "Three dimensional phase contrast angiography," Magn. Reson. Med. **9**, 139–149 (1989).

[4]C. L. Dumoulin, E. K. Yucel, P. Vock, S. P. Souza, F. Terrier, F. L. Steinberg, and H. Wegmuller, "Two- and three-dimensional phase contrast MR angiography of the abdomen," J. Comput. Assist. Tomogr. **14**, 779–784 (1990).

[5]C. L. Dumoulin, S. P. Souza, R. D. Darrow, N. J. Pelc, W. J. Adams, and S. A. Ash, "Simultaneous acquisition of phase- contrast angiograms and stationary-tissue images with Hadamard encoding of flow-induced phase shifts," J. Magn. Reson. Imag. **1**, 399–404 (1991).

[6]R. Hausmann, J. S. Lewin, and G. Laub, "Phase-contrast MR angiography with reduced acquisition time: New concepts in sequence design," J. Magn. Reson. Imag. **1**, 415–422 (1991).

[7]D. G. Nishimura, A. Macovski, and J. M. Pauly, "Magnetic resonance angiography," IEEE Trans. Med. Imag. **MI- 5**, 140–151 (1986).

[8]N. J. Pelc, M. A. Bernstein, A. Shimakawa, and G. H. Glover, "Encoding strategies for three-direction phase-contrast MR imaging of flow," J. Magn. Reson. Imag. **1**, 405–413 (1991).

[9]N. J. Pelc, R. J. Herfkens, A. Shimakawa, and D. R. Enzmann, "Phase contrast cine magnetic resonance imaging," Magn. Reson. Q. **7**, 229–254 (1991).

[10]G. B. Pike, C. H. Meyer, T. J. Brosnan, and N. J. Pelc, "Magnetic resonance velocity imaging using a fast spiral phase contrast sequence," Magn. Reson. Med. **32**, 476–483 (1994).

[11]M. A. Bernstein, M. Grgic, T. J. Brosnan, and N. J. Pelc, "Reconstruction of phase contrast, phased array multicoil data," Magn. Reson. Med. **32**, 330–334 (1994).

[12]N. J. Hangiandreou, P. J. Rossman, and S. J. Riederer, "Analysis of MR phase-contrast measurements of pulsatile velocity waveforms," J. Magn. Reson. Imag. **3**, 387–394 (1993).

[13]R. L. Wolf, R. L. Ehman, S. J. Riederer, and P. J. Rossman, "Analysis of systematic and random error in MR volumetric flow measurements," Magn. Reson. Med. **30**, 82–91 (1993).

[14]T. E. Conturo and B. H. Robinson, "Analysis of encoding efficiency in MR imaging of velocity magnitude and direction," Magn. Reson. Med. **29**, 134–138 (1992).

[15]T. E. Conturo and G. D. Smith, "Signal-to-noise in phase angle reconstruction: Dynamic range extension using phase reference offsets," Magn. Reson. Med. **15**, 420–437 (1990).

[16]S. M. Song, S. N. Napel, G. H. Glover, and N. J. Pelc, "Noise reduction in three-dimensional phase-contrast MR velocity measurements," J. Magn. Reson. Imag. **3**, 587–596 (1993).

[17]A. Caprihan and M. V. Icenogle, "A weighted least-squares method for nuclear magnetic resonance velocity imaging," Magn. Reson. Med. **29**, 512–520 (1993).

[18]A. T. Lee, G. B. Pike, and N. J. Pelc, "Three-point-phase contrast velocity measurements with increased velocity-to-noise ratio," Magn. Reson. Med. **33**, 122–126 (1995).

[19]S. O. Rice, "Mathematical analysis of random noise," Bell Syst. Tech. J. **24**, 46–156 (1945).

[20]W. A. Edelstein, P. A. Bottomley, and L. M. Pfeifer, "A signal-to-noise calibration procedure for NMR imaging systems," Med. Phys. **11**, 180–185 (1984).

[21]R. M. Henkelman, "Measurement of signal intensities in the presence of noise in MR images," Med. Phys. **12**, 232–233 (1985).

[22]M. A. Bernstein, D. M. Thomasson, and W. H. Perman, "Improved detectability in low signal-to-noise ratio magnetic resonance images by means of a phase-corrected real reconstruction," Med. Phys. **16**, 813–817 (1989).

[23]D. C. Noll, D. G. Nishimura, and A. Macovski, Homodyne detection in magnetic resonance imaging," IEEE Trans. Med. Imag. **MI-10**, 154–163 (1991).
[24]C. W. Helstrom, *Statistical Theory of Signal Detection* (Pergamon, New York, 1960).
[25]W. C. Lindsey, "Error probability for incoherent diversity reception," IEEE Trans. Information Theory **IT-11**, 491–499 (1965).
[26]R. E. Ziemer and W. H. Tranter, *Principles of Communication*, 2nd ed. (Houghton Mifflin, Boston, 1985).
[27]A. Papoulis, *Probability, Random Variables, and Stochastic Processes*, 1st ed. (McGraw-Hill, New York, 1965).
[28]G. N. Watson, *Theory of Bessel Functions*, 2nd ed. (Cambridge University Press, Cambridge, 1945).
[29]A. Erdélyi, *Tables of Integral Transforms* (McGraw-Hill, New York, 1954), Vol. I, p. 328.
[30]M. Abramowitz and I. A. Stegun, in *Handbook of Mathematical Functions* (National Bureau of Standards, U.S. Government Printing Office, Washington, DC, 1964).
[31]A. H. Andersen, J. E. Kirsch, and S. Guarnieri, "Low-contrast detectability in phase contrast MR imaging," *Proceedings of the Society of Magnetic Resonance Medicine*, 12th Annual Meeting, 1993, p. 709.
[32]G. McGibney and M. R. Smith, "An unbiased signal-to-noise ratio measure for magnetic resonance images," Med. Phys. **20**, 1077–1078 (1993).
[33]H. Gudbjartsson and S. Patz, "The Rician distribution of noisy MRI data," Magn. Reson. Med. **34**, 910–914 (1995).
[34]D. G. Brown and S. J. Riederer, "contrast-to-noise ratios in maximum intensity projection images," Magn. Reson. Med. **23**, 130–137 (1992).
[35]A. Erdélyi, in Ref. 29, p. 197.
[36]J. Marcum, "A statistical theory of target detection by pulsed radar," Math. Appendix, Report RM-753, Rand Corporation, 1948. Reprinted in IRE Trans. on Information Theory **IT-6**, 59–267 (1960).
[37]H. L. Van Trees, *Detection, Estimation, and Modulation Theory* (Wiley, New York, 1968), Part I.
[38]S. O. Rice, "Mathematical analysis of random noise," Bell Sys. Tech. J. **23**, 282–332 (1944). Reprinted by N. Wax, *Selected Papers on Noise and Stochastic Processes* (Dover, New York, 1954).